Real-time Moiré Interferometry

by H.S. Johnson, J.A. Gilbert, D.R. Matthys and T.D. Dudderar

ABSTRACT—A high-frequency moiré interferometric technique to continuously monitor in-plane surface displacement is presented. This technique employs fiber optics and a thermoplastic device to holographically record the initial carrier pattern produced on the surface of a test specimen. The carrier is modulated as the specimen deforms and moiré fringes, indicative of in-plane displacement, are observed in real time. Unwanted holointerferometric patterns are eliminated by appropriately adjusting the polarization of the reference wavefront. This paper describes a demonstration of the real-time technique as applied to the study of deformations in a notched beam subjected to three-point loading.

Introduction

High-frequency moiré interferometry is a highly sensitive full-field optical method useful for measurement of surface displacement.[1-3] The technique requires that a reflective high-frequency phase-type grating be transferred from a mold to the surface of the specimen. The mold is produced by exposing a photographic plate to the standing wave interference pattern produced at the intersection of two plane coherent wavefronts. Photographic processing and drying of the plate results in nonuniform shrinkage of the gelatin, producing a regularly corrugated mold shaped by the pattern of equispaced straight interference fringes. A thin film of reflective material is deposited on the surface of the mold in a vacuum chamber. This coated surface is then epoxied to the surface of the test specimen. Once the epoxy has cured the mold is removed, leaving a reflective, high-frequency phase grating on the test surface. When appropriately illuminated, the interference of the deposited grating with a reference grating having twice the spatial frequency yields a moiré pattern that can be analyzed to measure a selected component of surface displacement.

In practice, aberrations and preload prevent the specimen grating from being perfect (i.e., composed of perfectly straight, uniformly spaced corrugations), and a few fringes may be observed in the initial field when it is interrogated by the reference grating. This interrogation process may also contribute to the initial fringe pattern if the wavefronts of the two interfering beams used to create the reference grating are themselves not perfectly plane. Fortunately, introducing a carrier fringe pattern prior to loading permits these initial 'no-load' fringes to be optically subtracted from the load-induced displacement fringe pattern. There are two conditions[4] in which this subtraction may not be necessary: (1) when the initial 'no-load' fringe pattern is sparse but the full-load pattern has high fringe density, or (2) when the field of view has been magnified to such an extent that the initial pattern, as seen in the field of view, is a fraction of a fringe order. Only cases that satisfy one of these conditions have been studied in 'real time' (where the investigator is able to continuously monitor and evaluate full-field displacement at any point during the loading process); other cases involving relatively slight loading, and consequently only a modest number of fringes in the final state, have required that a double-exposure technique be used to optically remove the initial fringes from the field of view.

This study shows that holographic techniques can be used to store the initial carrier pattern for real-time analysis in the most general case. Fiber-optic components are incorporated into the experimental set up used to obtain the mold and into the displacement recording system to provide greater flexibility and potential optical access to remote test locations.

Interferometric Moire

Analysis

In high-frequency moiré interferometry the surface displacement is related to the moiré fringe pattern by the equation

$$U = (1/f)N \tag{1}$$

H.S. Johnson (SEM Member) is Graduate Student, and J.A. Gilbert (SEM Member) is Professor, Department of Mechanical Engineering, University of Alabama-Huntsville, Huntsville, AL 35899. D.R. Matthys (SEM Member) is Professor, Department of Physics, Marquette University, Milwaukee, WI 53233. T.D. Dudderar (SEM Fellow) is Member, Technical Staff, AT&T Bell Laboratories, Room 1A-105, 600 Mountain Avenue, Murray Hill, NJ 07974-2070.

Paper was presented at the 1986 SEM Spring Conference on Experimental Mechanics, held in New Orleans, LA on June 8-13.

Original manuscript submitted: August 1986. Final manuscript received: October 25, 1988.

where U is the displacement component measured perpendicular to the lines in the reference grating, f is the spatial frequency (the reciprocal of the distance between lines in the reference grating, usually defined as its pitch, p), and N is the order number assigned to fringes in the pattern. The reference grating (also called the virtual grating) is created in space by two interfering plane wavefronts (say W and W_1) of coherent light (see Fig. 1). The frequency of the interference lines, f, depends on the angle of intersection between the normals to the wavefronts (shown as 2α) and is characterized by the equation

$$f = (2 \sin \alpha)/\lambda \tag{2}$$

where λ is the wavelength of the incident light.

The substitution of eq (2) into eq (1) gives an expression for the in-plane displacement component, U, measured in a direction perpendicular to the lines in the reference grating,

$$U = N\lambda/2 \sin \alpha \tag{3}$$

in terms of the fringe-order number, N, the wavelength of light, and the angle of wavefront interference.

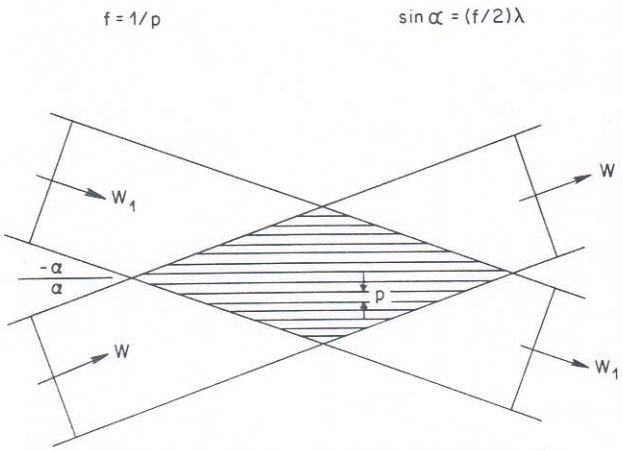

Fig. 1—Interference zone of two-plane wavefronts of coherent light

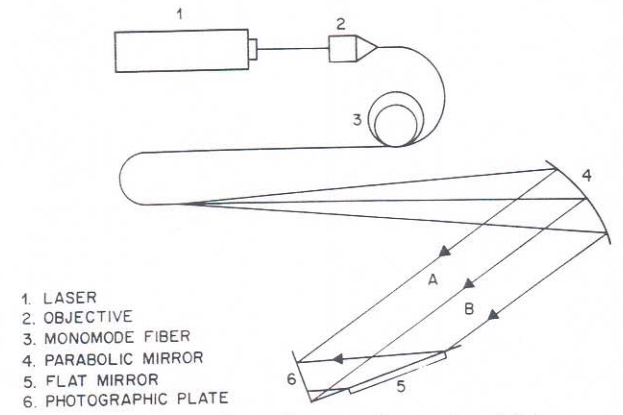

Fig. 2—Optical configuration used to produce high-frequency mold

Mold and Grating Production

Figure 2 shows the optical configuration used to produce the mold for the high-frequency grating. The flat mirror and photographic plate were illuminated by a collimated beam of argon-ion laser light (wavelength = 514.5 nm) generated by positioning the exit end of the monomode fiber five-deg off-axis in the focal plane of the parabolic mirror.* The resulting collimated beam of coherent light was used to illuminate the photographic plate both directly (beam A) and reflected off a flat mirror (beam B). In the set up shown in Fig. 2 each beam made an angle of 18 degrees with respect to the normal to the photographic plate. This configuration produced a virtual grating of equispaced vertical lines with a spatial frequency [governed by eq (2)] of approximately 1200 ℓ/mm.

After a first simultaneous exposure to beams A and B, the photographic plate was rotated 90 degrees around an axis normal to the surface and exposed a second time. This procedure produced a cross grating necessary for complete in-plane displacement analysis (although the present investigation focuses on recording a single displacement component).

Commercially available high-resolution photographic plates were used to record the phase grating. Exposures were made using the energy-controlled mode of the electronic shutter system. A light detector was placed in the collimated light beam outside of the field used to illuminate the photographic plate. The light intensity falling on the detector was scaled by an appropriate sampling factor which related the intensity monitored by the detector to that actually illuminating the photographic plate. The system was then operated to automatically assure exposures of optimum† integrated intensity.

Aluminum and gold have been shown to be good reflective mold overcoats because of their high reflectivity as thin films, low adhesion to the developed plate, and resistance to tarnishing.[4] Since the availability and cost of aluminum made it more desirable for testing, an aluminum overcoat approximately 1000 angstroms thick (50-percent reflectance) was vapor deposited on the plate in an environmentally controlled chamber. As illustrated in Fig. 3 and discussed in the Appendix, this aluminum grating was then transferred to the surface of the specimen shown in Fig. 4.

Experimental

Set Up

Figure 5 shows the experimental set up used to observe and record real-time moiré interferograms. The light beam from an argon-ion laser was split into two parts to form the object illumination and reference beams required for holographic recording. Each beam was launched into a separate single-mode step-index fiber[5,6] used to reduce stray illumination, improve flexibility and simplify the

In conventional practice, a principled effort must be made to minimize the angle between (1) the central ray of the diverging beam illuminating the parabolic mirror and (2) the propagation direction of the resulting collimated beam in order to optimize its planarity and assure a minimum initial fringe pattern. However, in the present case this restriction may be somewhat relaxed because, as will be shown, holographic techniques can be used to effectively cancel any such unwanted initial fringe pattern that might otherwise develop.

†*It was found that two exposures, of 1100 ergs/sq cm each, produced a cross grating with the largest first-order transmission diffraction efficiency.*

optical system. The exit end of the object illumination fiber was placed at the focal point of a parabolic mirror (2-m focal length, 0.41-m diameter), producing a wide collimated beam of coherent light. The parabolic mirror directed this object beam towards the specimen holder assembly where a flat mirror was positioned at 90 degrees to the model. This portion of the optical set up was identical to that used to generate the mold. The frequency of the virtual grating formed by the interference of the direct beam, A, and the reflected beam, B, was controlled by rotating the entire assembly about a vertical axis through the intersection between the specimen and the flat mirror. The orientation of the assembly was chosen to interrogate the specimen with a virtual grating having a frequency twice that of the real grating.

The specimen was placed in its holder under a slight preload. After rotating the assembly the specimen grating was oriented such that the +1 diffraction order of beam A coincided with the −1 diffraction order of beam B. With this alignment, light was diffracted in a direction normal to the surface as illustrated in Fig. 6 (extracted from Ref. 4). The remaining optical components were positioned along this direction as follows. (1) A linear polarizer was placed in the path of the diffracted wavefronts (see again Fig. 5) so as to polarize them vertically for maximum holographic diffraction efficiency. (2) These polarized wavefronts passed through a 38.1-mm diameter imaging lens of 375-cm focal length positioned 56.25 cm from the test surface to produce a magnification of two at the image plane. (3) A thermoplastic holographic recording device was placed normal to the direction of propagation at a location 15 cm behind the focal point of the lens. The diffracted wavefronts were stored holographically, and real images of the object and reconstructed holograms were recorded in the image plane on Polaroid or regular film.

Light exiting from the reference fiber passed through a half-wave plate and polarizer before illuminating the thermoplastic holographic plate. The half-wave plate and polarizer combination provided variable light transmission in a preferred direction of polarization while a light detector (not shown in Fig. 5) was mounted behind the thermoplastic plate to enable exposures to be regulated automatically using the electronic shutter system in an energy-controlled mode.

Procedure and Results

The notched beam specimen was placed in the loading frame with its longitudinal axis oriented horizontally as shown in Fig. 7. A carrier fringe pattern was created by introducing a linear mismatch between the specimen and

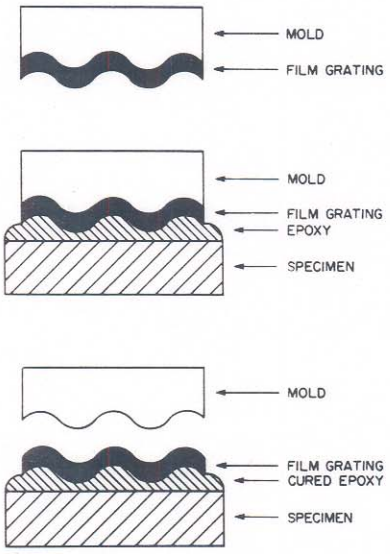

Fig. 3—The grating transfer from mold to specimen surface

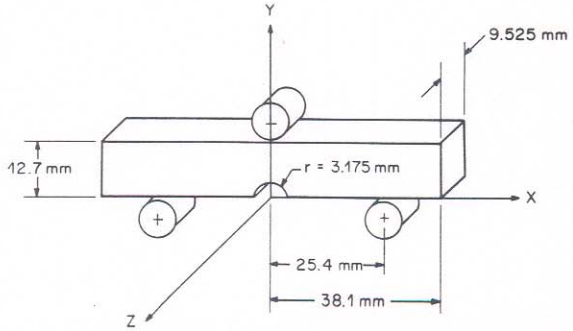

Fig. 4—Notched beam specimen

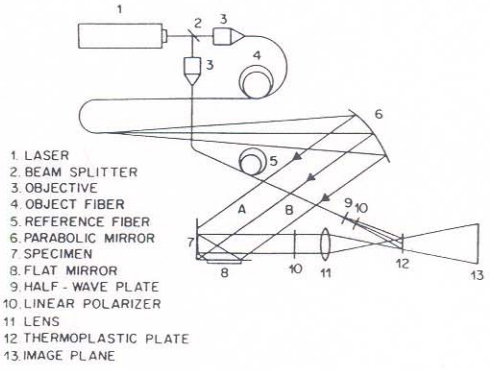

Fig. 5—Experimental setup

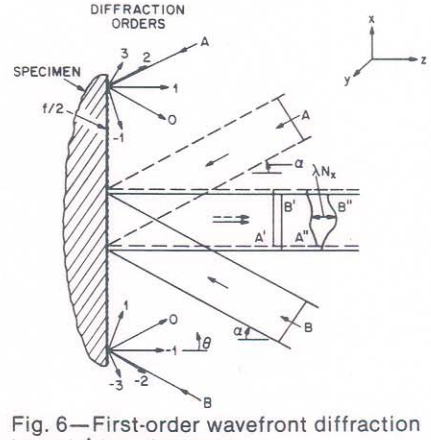

Fig. 6—First-order wavefront diffraction in moiré interferometry

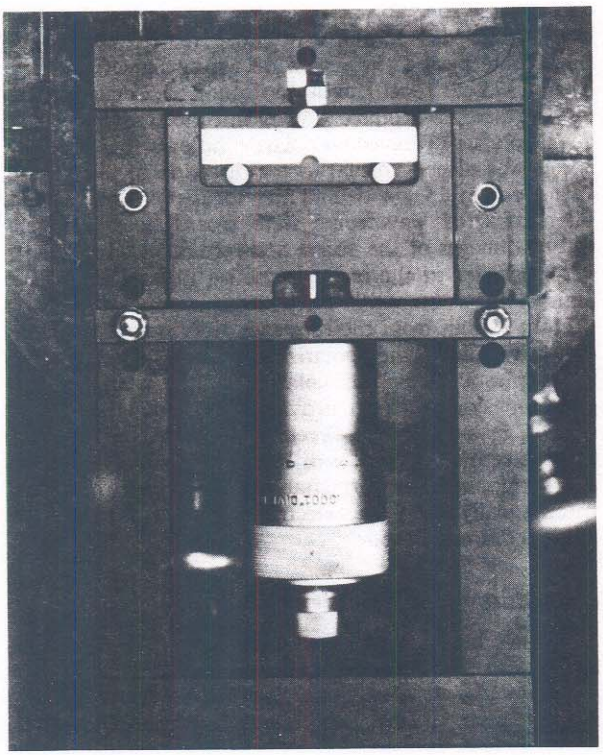

Fig. 7—Photograph of notched beam in loading frame

virtual gratings. Ideally, carrier fringes should be straight lines of equal density. Unfortunately, however, an initial preload was required to hold the model in place. This initial deformation, coupled with irregularities in the specimen grating, distorted the carrier fringe pattern, especially in the region of high strain (near the notch) as shown in Fig. 8. A hologram of the carrier pattern was recorded with polarizations of object and reference beams aligned in the vertical direction. Relative intensities of the two beams were adjusted using the variable density beam splitter. A holographic reconstruction of the object surface with the initial carrier fringe pattern was then photographed in the image plane by blocking the object beam and suitably illuminating the hologram (again see Fig. 8).

A real-time response was observed when the notched beam was loaded by displacing the lower supports. Figure 9 shows the modulated carrier pattern with the lower supports displaced 7.62×10^{-3} mm (0.0003 in.) upwards. In this case the holographic reference beam was blocked so as to display only the loaded state. When the initial and the modulated states were reconstructed simultaneously, two holointerferometric fringe patterns (resulting from the dual-beam illumination) and two sets of carrier fringes (caused by the superposition of the two diffracted wavefronts in the loaded and unloaded condition) appeared, resulting in a combination of fringe patterns far too complicated to analyze. In other words, because A & B' associated with the preload condition and A & B associated with the real-time final load condition are mutually coherent, they will usually generate an excessively complicated four-beam interference pattern if they are combined in the recording plane. However, each holointerferometric fringe pattern can be reconstructed independently by blocking either A, the reflected beam, or

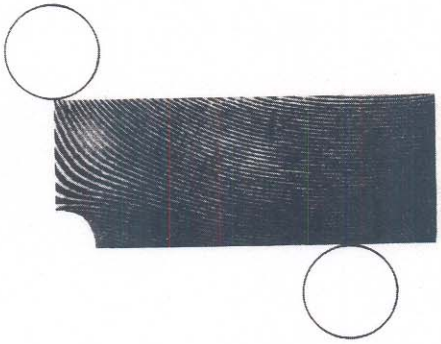

Fig. 8—Initial high-frequency moiré interferometric carrier pattern

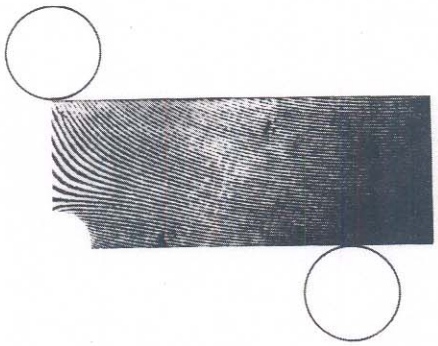

Fig. 9—Modulated high-frequency moiré interferometric carrier pattern

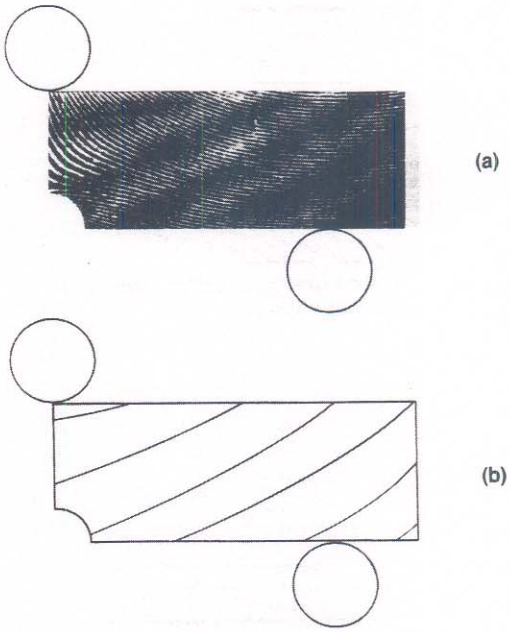

Fig. 10—Holointerferometric fringe pattern produced by illumination with direct beam A (a) superimposed on the initial high-frequency moiré interferometric carrier and a (b) schematic of holointerferometric fringe loci

B, the direct beam. Figures 10 and 11 show the patterns recorded with beams A', B' and A or A', B′ and B, respectively. Of course, each holointerferometric fringe pattern is superimposed on the initial carrier.

The holointerferometric fringe patterns are characterized by the expression

$$\underline{g} \cdot \underline{d} = n_d \lambda \tag{4}$$

where g is the sensitivity vector $(\underline{k}_2 - \underline{k}_1)$, $\underline{k}_1$ and $\underline{k}_2$ are unit vectors in the illumination and observation directions respectively, $\underline{d}$ is the displacement at the surface observation point, n_d is the fringe-order number, and λ is the wavelength. The sensitivity vector, $\underline{g}_A$, of the pattern recorded with direct illumination (beam A) is described by

$$\underline{g}_A = \underline{k}_2 - (-\sin\alpha\underline{i} - \cos\alpha\underline{k}) \tag{5}$$

while the sensitivity vector $\underline{g}_B$, of the pattern recorded with reflected illumination (beam B) is described by

$$\underline{g}_B = \underline{k}_2 - (\sin\alpha\underline{i} - \cos\alpha\underline{k}) \tag{6}$$

where α is the angle between the illumination beams and the normal to the object surface, and $\underline{i}$, $\underline{k}$ are unit vectors along the x, z axes shown in Fig. 4.

These can be substituted into eq (4), giving

$$\begin{aligned} \underline{g}_A \cdot \underline{d} &= n_A \lambda \\ \underline{g}_B \cdot \underline{d} &= n_B \lambda \end{aligned} \tag{7}$$

Their superposition is represented by the difference between these equations

$$n_d \lambda = (\underline{g}_A - \underline{g}_B) \cdot \underline{d} \tag{8}$$

Substituting eqs (5) and (6) into eq (8),

$$n_d \lambda = U(2 \sin\alpha) \tag{9}$$

where U is the in-plane displacement component along the longitudinal axis of the beam. Equation (9) is equivalent to eq (3) which governs the patterns obtained with moiré interferometry.

This situation has been investigated previously[7-9] and is classified as holographic-moiré analysis. In general, sufficiently large additional phase changes could be introduced between exposures to create high fringe densities in each of the two component patterns (one created by each illumination) so that they interfere and produce holointerferometric moiré fringes. However, no additional phase changes have been added to the component patterns in the present investigation, and the holointerferometric fringe patterns (shown in Figs. 10 and 11) have insufficient fringe densities to produce the moiré effect upon superposition (see Fig. 12). However, holointerferometric moiré fringes can be constructed graphically as shown in Fig. 13 for subsequent comparison with those obtained from high-frequency moiré interferometry.

Fortunately, the holointerferometric component patterns are not required to make the desired real-time measure-

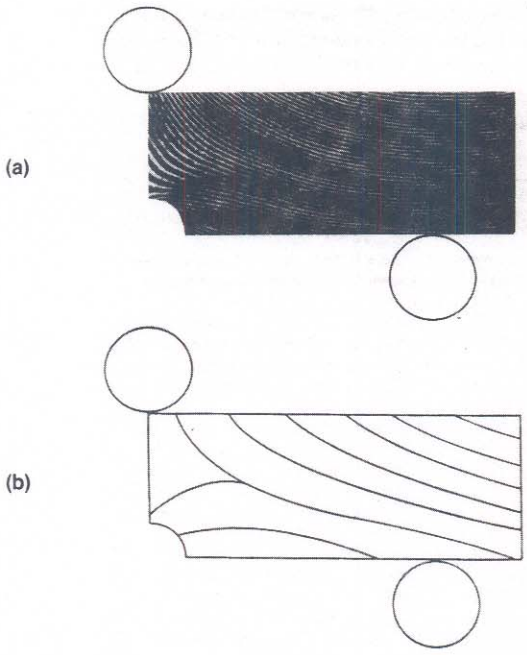

Fig. 11—Holographic pattern produced by illumination with reflected beam B
(a) superimposed on the initial high-frequency moiré interferometric carrier and a (b) schematic of holographic fringe loci

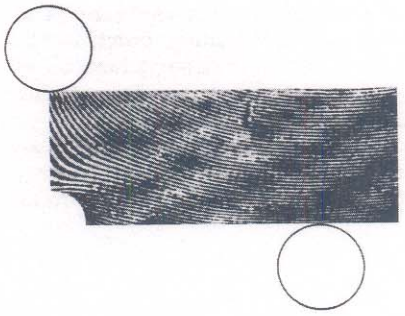

Fig. 12—Holographic pattern produced by dual-beam illumination superimposed with initial and modulated high-frequency moiré interferometric carriers

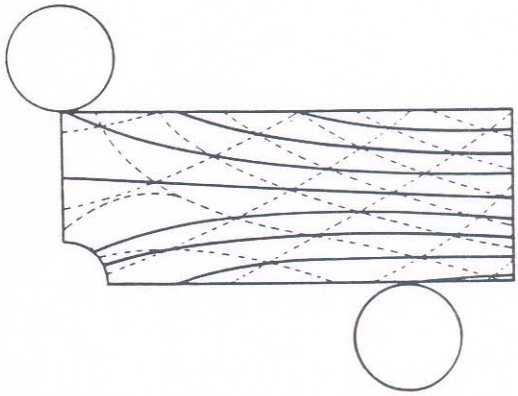

Fig. 13—Geometrically constructed holographic-moiré fringes

ments of in-plane displacements. Moreover, they can easily be eliminated by reconstructing the carrier pattern (and each of the initial holograms) using horizontally polarized light (produced by rotating the half-wave plate and polarizer in the reference beam). In this case, the vertically polarized object beam and the horizontally polarized reference beam will produce no interference and no real-time holointerferometric fringes. However, the initial moiré interferometric carrier is still reconstructed holographically. This pattern may then be superimposed on the deformed carrier, which depends only upon the interference between the two object wavefronts diffracted from the specimen in its loaded condition. A similar approach was followed by Chiang and Li[10] in an application to real-time laser speckle photography.

Real-time interferometric moiré fringes can now be photographed in the image plane as shown in Fig. 14. The pattern is indicative of displacement in the U direction (along the longitudinal axis of the beam). Fringe numbers are assigned starting with zero at the top center support and the displacement can be calculated using eq (1) (f = 2400 ℓ/mm). As expected, the fringe loci agree well with those constructed in Fig. 13.

Conclusion and Recommendations

Real-time moiré interferograms have been recorded using a holocamera to store information corresponding to the 'undeformed' condition of a structural component. The main advantage of this approach over the earlier double-exposure technique is that here the investigator is able to continuously monitor and evaluate full-field displacement during the loading process. This could be extremely important in dynamic situations where a time history must be established: for example, in monitoring crack initiation and growth.

In future research, the visibility of real-time moiré fringes could be enhanced using a fiber-optic imaging bundle with a resolution sufficient to transmit the moiré, but too low to resolve the high-frequency carriers. This filtered real-time image could be transferred to a video system for automated analysis.

This procedure (incorporating high-resolution photoelectronic recording, data acquisition, digitization, computer-based file manipulation, numerical correlation and graphics display routines) would make quasi-real-time computerized numerical subtraction and/or addition of individual carrier fringe fields a possible alternative to optical superposition. Interpretation of surface motion could be accomplished after completing an experimental procedure by choosing and numerically comparing any two carrier fringe patterns, as recorded on video tape. This would extend the range over which displacement could be measured and would eliminate the need for subjective evaluations of fringe patterns by investigators.

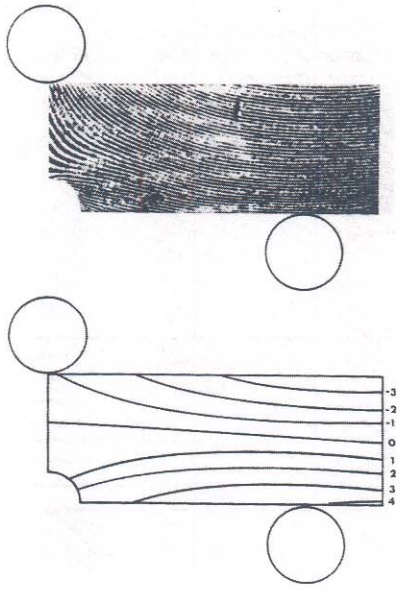

Fig. 14—Real-time interferometric moiré pattern and a (b) schematic of real-time interferometric moiré fringe

Acknowledgments

The authors gratefully acknowledge the support of the Army Research Office (Contract Nos. DAAG 29-84-K-0183 and DAAL 03-86-K-0014), the Center for Applied Optics at the University of Alabama in Huntsville, Marquette University, and AT&T Bell Laboratories. Special thanks are extended to Dan Post and his group at Virginia Polytechnic Institute for their many helpful discussions regarding moiré interferometry.

APPENDIX

The Mold Transfer Technique

A beam with dimensions shown in Fig. 4 was made of PSM-1 (a photoelastic material). After the surface was degreased with isopropanol, roughened with abrasive paper and cleaned with surface conditioner, a thin coat of epoxy was applied to the beam. The epoxied surface was carefully placed face down on the dust free, processed and aluminized photographic plate. After the epoxy cured overnight, the specimen was carefully pried from the plate and excess epoxy in the notched area and along the edges of the beam was removed by hand sanding and/or grinding on a fine-grit surface-preparation power wheel.

References

1. *Post, D., "Moiré Interferometry for Deformation and Strain Studies," Opt. Eng.,* **24** *(4), 663-667 (1985).*

2. *Basehore, M.L. and Post, D., "Displacement Fields (U, W) Obtained Simultaneously by Moiré Interferometry," Appl. Opt.,* **21** *(14), 2558-2562 (1982).*

3. *Post, D., Czarnek, R., Joh, D. and Wood, J.D., "Shear Strain Anomalies in Composite Beam Specimens by Moiré Interferometry," Proc. SEM Spring Conf. on Exp. Mech., 916-921 (June 1985).*

4. *Post, D., "Moiré Interferometry at VPI & SI,"* EXPERIMENTAL MECHANICS, **23** *(6), 203-210 (1983).*

5. *Dudderar, T.D. and Gilbert, J.A., "Real-time Holographic Interferometry Through Fiber Optics," J. Phys. E: Sci. Instr.,* **18**, *39-43 (1985).*

6. *Gilbert, J.A. and Dudderar, T.D., "Applications of Fiber Optics to Coherent Metrology for the Study of Material Deformations and Structural Mechanics," Army Symp. on Solid Mechanics, Newport, RI, 63-92 (Oct. 1984).*

7. *Sciammarella, C.A. and Gilbert, J.A., "A Holographic-moiré Technique to Obtain Separate Patterns for Components of Displacement,"* EXPERIMENTAL MECHANICS, **16** *(6), 215-220 (1976).*

8. *Hung, Y.Y. and Taylor, C.E., "Measurement of Surface Displacements Normal to Line of Sight by Holo-moiré Interferometry," J. Appl. Mech.,* **42** *E (1), 1-4 (1975).*

9. *Beranek, W.J. and Bruinsma, A.J.A., "Determination of Displacement and Strain Fields Using Dual-beam Holographic-moiré Interferometry,"* EXPERIMENTAL MECHANICS, **22** *(9), 317-323 (1982).*

10. *Chiang, F.P. and Li, Q.B., "Real-time Laser Speckle Photography," Appl. Opt.,* **23** *(24), 4469-4470 (1984).*